PCCP

Accepted Manuscript

This is an *Accepted Manuscript*, which has been through the Royal Society of Chemistry peer review process and has been accepted for publication.

Accepted Manuscripts are published online shortly after acceptance, before technical editing, formatting and proof reading. Using this free service, authors can make their results available to the community, in citable form, before we publish the edited article. We will replace this *Accepted Manuscript* with the edited and formatted *Advance Article* as soon as it is available.

You can find more information about *Accepted Manuscripts* in the Information for Authors.

Please note that technical editing may introduce minor changes to the text and/or graphics, which may alter content. The journal's standard Terms & Conditions and the Ethical guidelines still apply. In no event shall the Royal Society of Chemistry be held responsible for any errors or omissions in this *Accepted Manuscript* or any consequences arising from the use of any information it contains.

ROYAL SOCIETY OF CHEMISTRY

www.rsc.org/pccp

Complexation dynamics of CH_3SCN and Li^+ in acetonitrile studied by two-dimensional infrared spectroscopy

YoungAh Kwon[1] and Sungnam Park[1,2*]

[1]Department of Chemistry, Korea University, Seoul 136-701, Korea.

[2]Multidimensional Spectroscopy Laboratory, Korea Basic Science Institute, Seoul 136-713, Korea.

[*]Authors to whom correspondence should be addressed.

Email address: spark8@korea.ac.kr

Abstract

Ion-molecule complexation dynamics were studied with CH_3SCN and Li^+ in acetonitrile by vibrationally probing the nitrile stretching vibration of CH_3SCN. The nitrile stretching vibration of CH_3SCN has a long lifetime (T_1=~90 ps) and its frequency is significantly blue-shifted when CH_3SCN is bound with Li^+ ion to form $CH_3SCN\cdots Li^+$ complex in acetonitrile. Such spectral properties enable us to distinguish free CH_3SCN and $CH_3SCN\cdots Li^+$ complex in solutions and measure their dynamics occurring on hundred picosecond timescales. For the complexation between CH_3SCN and Li^+ in acetonitrile, the change in enthalpy ($\Delta H = -7.17$ kJ mol^{-1}) and the change in entropy ($\Delta S = -34.4$ J K^{-1} mol^{-1}) were determined by temperature-dependent FTIR experiments. Polarization-controlled infrared pump-probe (IR PP) spectroscopy was used to measure the population decay and orientational dynamics of free CH_3SCN and $CH_3SCN\cdots Li^+$ complex. Especially, the orientational relaxation of $CH_3SCN\cdots Li^+$ complex was found to be almost 3 times slower than those of free CH_3SCN because Li^+ ion strongly interacts with the neighboring solvents. Most importantly, the complexation dynamics of CH_3SCN and Li^+ in acetonitrile were successfully measured in real time by 2DIR spectroscopy for the first time and the dissociation and association time constants were directly determined by using the two-species exchange kinetic model. Our experimental results provide a comprehensive overview of the ion-molecule complexation dynamics in solutions occurring under thermal equilibrium conditions.

I. Introduction

Electrolyte solutions are very common and their applications are found in many different research areas, such as Li batteries, solar cells, aqueous ionic solutions, and so on. The properties of electrolyte solutions are characterized by the ion-ion interactions and ion-molecule interactions.[1] Such interactions in electrolyte solutions play important roles in determining the diffusion of ions, ion pairing, and ionic solvation. In electrolyte solutions, oppositely charged ions (cations and anions) associate to form different types of ion pairs (i.e., contact ion pairs, solvent-shared ion pairs, and solvent-separated ion pairs) while ion pairs dissociate into free ions.[2] Recently, ion pairing dynamics in electrolyte solutions were successfully studied by two-dimensional infrared (2DIR) spectroscopy and were found to occur on a few hundred picosecond timescales.[3, 4] In addition, ions and dipolar molecules are bound to form ion-molecule complexes by the ion-dipole interactions. Ion-molecule complexes dissociate into the corresponding ions and molecules when the ion-dipole interactions are thermally perturbed. The timescales of such ion-molecule complexation dynamics are experimentally unknown. Direct measurements of ion-molecule complexation dynamics occurring under thermal equilibrium conditions have been experimentally challenging. Here, 2DIR spectroscopy was successfully applied to directly investigate the ion-molecule complexation dynamics. In fact, 2DIR spectroscopy has been proved to be a powerful experimental method to study thermally-induced structural dynamics in solutions occurring on picosecond timescales and has been applied to study many interesting and fundamental molecular systems.[3-19]

In this work, the complexation dynamics of Li^+ and CH_3SCN in acetonitrile were comprehensively studied. To vibrationally probe the complexation dynamics by 2DIR spectroscopy, CH_3SCN was chosen as a dipolar molecule because its nitrile stretching vibration was found to have a long lifetime (T_1=~90 ps) in acetonitrile which allowed us to measure the complexation dynamics occurring on hundred picosecond timescales. The nitrile stretching

vibrations have been used as a vibrational probe for many applications.[20-23] In the case of CH_3SCN, sulfur atom behaves like a thermal insulator so that the nitrile stretching vibration can have a relatively long vibrational lifetime.[24] In addition, Li^+ ion was used because it is known to be one of the most important cations commonly used in rechargeable batteries[25-27] and high-performance capacitors.[28-30] The thermodynamic properties of the complexation equilibrium of Li^+ and CH_3SCN in acetonitrile were studied by temperature-dependent FTIR spectroscopy. IR PP spectroscopy was used to measure the population and orientational relaxation dynamics of free CH_3SCN and $CH_3SCN\cdots Li^+$ complex. Most interestingly, the complexation dynamics of Li^+ and CH_3SCN in acetonitrile were able to be successfully measured in real time by 2DIR spectroscopy. Both IR PP and 2DIR data were simultaneously fitted to the two-species exchange kinetic model and the dissociation and association rate constants were directly determined.

II. Experimental methods

A. Sample preparation

$LiClO_4$, acetonitrile (CH_3CN), and methyl thiocyanate (CH_3SCN) were purchased from Sigma-Aldrich. A mixture of CH_3SCN and CH_3CN with a 1:10 molar ratio was prepared and the concentration of CH_3SCN was 1.69 M. The sample solutions with different concentrations of $LiClO_4$ salt were prepared by directly dissolving $LiClO_4$ salt in the mixture of CH_3SCN and CH_3CN. In solutions, $LiClO_4$ dissociates fully into Li^+ and ClO_4^- and then Li^+ ions are bound with CH_3SCN to form $CH_3SCN\cdots Li^+$ complexes. For IR experiments, the sample solutions were housed in a home-made IR cell with two 3 mm thick CaF_2 windows. The optical path length of the sample cell was set to be 12 μm by a Teflon spacer.

B. FTIR spectroscopy

All FTIR spectra were collected by a Varian 640-IR spectrometer with a ~0.5 cm^{-1} resolution. For temperature-dependent FTIR experiments, the cell was connected to a temperature controller (PIKE Technologies, USA) with a K-type thermocouple and rod-heater which could allow us to raise the temperature of the sample solution by 0.1 °C. Temperature-dependent FTIR spectra were measured from 25 to 65 °C with an interval of 5 °C. At a given temperature, the sample solution was kept for at least 15 minutes before its FTIR spectrum was taken to ensure the thermal equilibrium was established. After the temperature-dependent FTIR experiments were finished, the sample solution was quickly cooled down to the initial temperature (25 °C) by using a fan. FTIR spectrum of the sample solution was measured before and after the experiment to check any photo-degradation or thermal degradation of the sample during the experiments. We found that there was no significant degradation of the sample.

C. 2DIR and IR PP spectroscopy

Our femtosecond laser system and time-resolved spectrometers have been described in detail elsewhere.[31-33] Briefly, a train of 800 nm pulses with ~45 fs duration and ~1.0 mJ per pulse is generated by a Ti:sapphire oscillator (Tsunami, Spectra-Physics) and regenerative amplifier (Spitfire, Spectra-Physics) laser system operating at 1 kHz. The 800 nm pulses are used to pump an optical parametric amplifier (OPA, Spectra-Physics) to produce near-IR pulses which are used to generate mid-IR pulses centered at ~2170 cm^{-1} in a 0.5 mm thick $AgGaS_2$ crystal (Type II) by difference frequency generation. The power spectrum of the mid-IR pulses has a Gaussian envelope with a ~260 cm^{-1} bandwidth (full width at half-maximum). The CaF_2 plates with different thicknesses are used to compensate for the linear dispersion introduced by other dielectric materials in the setup including a Ge Brewster plate and ZnSe beam splitters. The mid-IR pulses are nearly transform-limited at the sample position.

The principles and experimental details of two-dimensional infrared (2DIR) spectroscopy have been described elsewhere.[34-41] Three mid-IR pulses are focused with a 90 degree off-axis parabolic mirror (f.l.=100 mm) onto the sample in a box-car geometry. After the sample, the beams are collimated with another 90 degree off-axis parabolic mirror (f.l.=100 mm). The spot size of the IR beams at the sample position is less than 100 μm in diameter. The relative time-delays among three incident IR pulses are varied with computer-controlled linear translational stages. The signal is emitted from the sample in a unique phase-matched direction and is overlapped with a local oscillator pulse for heterodyne detection. The heterodyned signal is dispersed through a spectrometer onto the 64-element mercury-cadmium-telluride (MCT) array detector with high speed data acquisition electronics (Infrared Associates and Infrared Systems Development Corp.). A small portion of the IR beam is sampled before the sample and is used as a reference beam to correct the fluctuation of the laser intensity during the experiments. In 2DIR experiments, there are three experimental time variables that can be controlled. The time-delay between the first and second pulses is the coherence evolution time (τ), the time delay between the second and third pulses is the waiting time (T_w), and the time-delay between the third pulse and the emitted signal is the detection time (t). The heterodyned 2DIR signal, $S(\tau, t; T_w)$, is collected by scanning τ at a fixed T_w, frequency-resolved by a spectrometer, and detected by the 64-element array detector. To obtain the 2DIR spectra at a given T_w, $S(\omega_\tau, \omega_t; T_w)$, Fourier transformation of the signal with respect to τ and t time periods should be performed. The spectrometer essentially performs the Fourier transform of the detection time (t) to generate the ω_t-dependent spectrum, while another Fourier transform is numerically performed for the evolution time (τ) after collecting the τ-dependent interferogram for each value of ω_t. This Fourier transformation provides the ω_τ-dependent spectrum. 2DIR spectra, $S(\omega_\tau, \omega_t; T_w)$, are therefore displayed with respect to the initial excitation frequency ω_τ and

final emission frequency ω_t at a given T_w. Purely absorptive 2DIR spectrum is obtained by using the dual scan method in which non-rephasing and rephasing 2DIR signals are measured separately by two different pulse sequences and are added together.[42]

For IR PP experiments,[40, 43] the IR pulses are split into the pump and probe beams with a 9:1 intensity ratio and are focused onto the sample. The probe beam is collimated after the sample and is dispersed through a spectrometer onto the 64-element MCT array detector. The IR PP signal $S(t)$ is collected by measuring the transmission of the probe beam through the sample by chopping the pump beam at 500 Hz. For a given delay time t, the IR PP signal is defined by $S(T) = [T_{\text{pump-on}} - T_{\text{pump-off}}](t) / T_{\text{pump-off}} = \Delta T(t) / T$ where T is the transmission of the probe beam. For polarization-controlled IR PP experiments, the wire-grid polarizers are placed in the pump and probe beam pathways before the sample and their polarization states are set to be 0° and 45° with respect to the normal to the optical table, respectively. A wire-grid analyzer polarizer on a motorized rotational stage is placed after the sample and the parallel and perpendicular polarizations of the probe beam are selectively measured by setting the analyzer polarizer to be 0° and 90° by the computer-controlled motorized rotational stage. The parallel and perpendicular IR PP signals, $S_{\parallel}(\omega_{\text{pr}}, t)$ and $S_{\perp}(\omega_{\text{pr}}, t)$, are consecutively measured for every two scans with the polarization of the probe beam parallel and perpendicular to that of the pump beam, respectively. In this work, 2DIR and IR pump–probe experiments were conducted at 22 °C.

III. Results and discussion

A. FTIR study

The nitrile (CN) stretching vibration of methyl thiocyanate (CH_3SCN) has a strong infrared absorption at 2158 cm^{-1} in acetonitrile.[44-46] Figure 1(A) displays the nitrile stretching band of CH_3SCN in acetonitrile at different concentrations of Li^+ ion (or $LiClO_4$). In Figure 1(A), the

high frequency peak at 2180 cm^{-1} appears upon addition of Li^+ ion. As the concentration of Li^+ ion is increased, the low frequency peak at 2158 cm^{-1} decreases gradually while the high frequency peak at 2180 cm^{-1} increases. The isosbestic point is observed at 2164.5 cm^{-1}. In acetonitrile, Li^+ ion is bound to CH_3SCN to form a $CH_3SCN\cdots Li^+$ complex and the nitrile stretching band of $CH_3SCN\cdots Li^+$ is significantly blue-shifted to 2180 cm^{-1}. Therefore, free CH_3SCN and $CH_3SCN\cdots Li^+$ complex are spectrally well distinct. Figure 1(B) shows the temperature-dependent FTIR spectra of the sample solution with 2.0 M Li^+ ion. As the temperature is increased, the low frequency peak decreases gradually and the high frequency peak gets red-shifted and its amplitude decreases. The complexation equilibrium between CH_3SCN and Li^+ is written as

$$CH_3SCN + Li^+ \underset{k_d}{\overset{k_a}{\rightleftharpoons}} CH_3SCN\cdots Li^+ \qquad (1)$$

where k_a and k_d are the association (or complexation) and dissociation rate constants, respectively. The mass balances are given by $[Li^+]_0 = [Li^+] + [CH_3SCN\cdots Li^+] = 2.0\ \mathrm{M}$ and $[CH_3SCN]_0 = [CH_3SCN] + [CH_3SCN\cdots Li^+] = 1.69\ \mathrm{M}$. The equilibrium constant K_{eq} is defined as $K_{eq} = [CH_3SCN\cdots Li^+]/([Li^+][CH_3SCN]) = k_a/k_d$. Here, the activity coefficients of each individual chemical species are not taken into account for the sake of simplicity. As shown in Figure 1(C), FTIR spectrum at a given temperature is decomposed into the nitrile stretching bands of free CH_3SCN and $CH_3SCN\cdots Li^+$ complex and the areas of the two peaks are obtained by numerical integration. In the FTIR spectrum, the absorbance which is written by the Beer's law (i.e., $Abs(\lambda) = \varepsilon(\lambda)bC$ where $\varepsilon(\lambda)$ is the extinction coefficient, b is the path length, and C is the concentration) is directly proportional to the peak area (PA), i.e., $\mathrm{PA} \propto Abs(\lambda)$. At a given temperature, the ratio of the peak areas is equal to the ratio of the concentrations, i.e., $\mathrm{PA}_{[CH_3SCN]}/\mathrm{PA}_{[CH_3SCN]_0} = [CH_3SCN]/[CH_3SCN]_0$ where $[CH_3SCN]_0$ and $[CH_3SCN]$ are the concentration of CH_3SCN in 0.0 and 2.0 M Li^+ solutions, respectively.

$[CH_3SCN] = PA_{[CH_3SCN]} / PA_{[CH_3SCN]_0} \times [CH_3SCN]_0$ is calculated from the ratio of the peak areas. After $[CH_3SCN]$ is determined, $[CH_3SCN \cdots Li^+] = [CH_3SCN]_0 - [CH_3SCN]$ and $[Li^+] = [Li^+]_0 - [CH_3SCN \cdots Li^+]$ are readily calculated by using the mass balances. In fact, the amplitude of the nitrile stretching band of free CH_3SCN is decreased with increasing the temperature, which results from the temperature-dependent transition dipole moment of the nitrile stretching band (see Figure S3 in the ESI). As the temperature is raised, $[CH_3SCN]/[CH_3SCN \cdots Li^+]$ is found to increase implying that that the dissociation of $CH_3SCN \cdots Li^+$ complex is more favored at higher temperatures. The equilibrium constant (K_{eq}) for the complexation equilibrium in Eq. (1) is calculated at each temperature by using the equilibrium concentrations of Li^+, CH_3SCN, and $CH_3SCN \cdots Li^+$. As shown in Figure 1(D), $\ln K_{eq}$ is plotted against $1/T$ (van't Hoff plot) and the changes in enthalpy and entropy for the complexation equilibrium in Eq. (1) are determined to be $\Delta H = -7.17$ kJ mol^{-1} and $\Delta S = -34.4$ J K^{-1} mol^{-1}, respectively. These results suggest that the formation of $CH_3SCN \cdots Li^+$ complex in acetonitrile should be an exothermic process and be entropically unfavorable in the experimental temperature range.

B. 2DIR study

Complexation dynamics between CH_3SCN and Li^+ in acetonitrile were measured by vibrationally probing the nitrile stretching vibrations by 2DIR spectroscopy. Figure 2 shows all the 2DIR spectra measured at a series of T_w times and the corresponding FTIR spectrum is plotted on the top. In Figure 2, the red peaks at $\omega_\tau = \omega_t = 2157$ cm^{-1} (Peak F) and at $\omega_\tau = \omega_t = 2180$ cm^{-1} (Peak C) on the diagonal axis (dotted lines) are positive resulting from the fundamental transitions originating from the ground state bleach (GSB, $\upsilon = 0 \rightarrow 1$) and stimulated emission (SE, $\upsilon = 0 \leftarrow 1$) of the nitrile stretching vibrations of free CH_3SCN and $CH_3SCN \cdots Li^+$ complex,

respectively. The blue peaks below the diagonal peaks are negative originating from the excited stated absorption (ESA, $\upsilon = 1 \rightarrow 2$) of the nitrile stretching vibrations and are red-shifted by their vibrational anharmonicities. In the 2DIR spectrum at T_w=1.0 ps, the two nitrile stretching bands of free CH_3SCN and $CH_3SCN\cdots Li^+$ complex are well separated. As T_w is increased, the cross-peaks (Peak X1, X2, and X3) grow gradually as indicated in the 2DIR spectrum at T_w=180 ps. Peak X1 (positive in sign) results from the complexation (association) process ($CH_3SCN + Li^+ \rightarrow CH_3SCN\cdots Li^+$). In fact, the negative $\upsilon = 1 \rightarrow 2$ transition of X1 is underneath Peak F. Positive Peak X2 and negative Peak X3 come from the dissociation process ($CH_3SCN + Li^+ \leftarrow CH_3SCN\cdots Li^+$). However, positive Peak X2 is significantly overlapped with the negative $\upsilon = 1 \rightarrow 2$ transition of the nitrile stretching vibration of $CH_3SCN\cdots Li^+$ and thus its amplitude is almost cancelled.

In our 2DIR experiments, the nitrile stretching vibrations of free CH_3SCN and $CH_3SCN\cdots Li^+$ complex are excited and vibrationally labeled at T_w=0 ps. At short T_w times, the two nitrile peaks on the diagonal axis in 2DIR spectra are dominantly observed. As T_w is increased, the diagonal peaks (F and C in Figure 2) decay as a result of the vibrational population and orientational relaxation, and the cross-peaks grow gradually due to thermally-induced complexation and dissociation processes presented in Eq. (1). In addition, the peaks in 2DIR spectra change from diagonally elongated to symmetrical shapes with increasing T_w time. Accordingly, 2DIR spectra evolve dynamically as a function of T_w time as shown in Figure 2. In principle, all the dynamic information on the molecular system under study can be extracted by analyzing the T_w-dependent 2DIR spectra. Generally, 2DIR signals can be collected only when the vibrational probes (i.e., the CN stretching vibrations) are on the excited states. In some cases, the lifetime of the vibrational probe limits the experimental dynamic range of the molecular system studied by 2DIR spectroscopy. In our present experiments, 2DIR spectra were

able to be successfully measured up to T_w=180 ps because of a long vibrational lifetime of the nitrile stretching vibration of CH_3SCN.

C. IR PP study

In IR PP experiments, a molecule is vibrationally excited to $\upsilon = 1$ state by a strong pump pulse and the relaxation of the vibrationally excited state is monitored by a weak probe pulse as a function of delay time between pump and probe pulses. The IR PP signal decays as a result of the vibrational population relaxation and orientational relaxation. Polarization-controlled IR PP experiments were carried out to selectively measure the population and orientational relaxation dynamics. It should be mentioned that in the case of our sample solution, the $\upsilon = 0 \rightarrow 1$ transition (2157 cm^{-1}) of the nitrile stretching vibration of CH_3SCN significantly was overlapped with the $\upsilon = 1 \rightarrow 2$ transition of the CN stretching vibration of $CH_3SCN\cdots Li^+$. We used the IR PP signals measured at ω_t=2180 cm^{-1} ($\upsilon = 0 \rightarrow 1$ transition) for $CH_3SCN\cdots Li^+$ and at ω_t=2133 cm^{-1} ($\upsilon = 1 \rightarrow 2$ transition) for CH_3SCN to obtain the population relaxation and orientational relaxation dynamics.

The vibrational population decay, $P(t)$, is obtained from the polarization-controlled IR PP signals by[38]

$$P(t) = S_{\parallel}(t) + 2S_{\perp}(t), \qquad (2)$$

where $S_{\parallel}(t)$ and $S_{\perp}(t)$ are the parallel and perpendicular IR PP signals, respectively. Figure 3(A) displays $P(t)$ measured at 2180 cm^{-1} for $CH_3SCN\cdots Li^+$ and at 2133 cm^{-1} for CH_3SCN, respectively. As shown in Figure 3(A), $P(t)$ is reasonably well described by a single exponential function, $P(t) = A\exp(-t/\tilde{T}_1)$, with $\tilde{T}_1 = 92 \pm 2$ ps for CH_3SCN and $\tilde{T}_1 = 78 \pm 2$ ps for $CH_3SCN\cdots Li^+$, respectively. Here, the tilde indicates an apparent lifetime. In the cases of the molecular systems with chemical exchange processes, IR PP signals also include the chemical

exchange dynamics and thus the time constants ($\tilde{T}_1$) determined above are not the true lifetimes of vibrational probes. The true vibrational lifetimes can be extracted by taking into account the chemical exchange processes included in the IR PP signals, which will be discussed in more detail in the next section.

The orientational anisotropy decay, $r(t)$, is related to the orientational correlation function $C_{or}(t)$ as,

$$r(t) = \frac{S_{\parallel}(t) - S_{\perp}(t)}{S_{\parallel}(t) + 2S_{\perp}(t)} = \frac{2}{5} C_{or}(t) \quad (3)$$

The orientational anisotropy decay, $r(t)$, is proportional to $C_{or}(t)$, which is the second-order Legendre polynomial ($P_2(x)$) of the transition dipole correlation function as, $C_{or}(t) = \left\langle P_2\left[\boldsymbol{\mu}(t)\cdot\boldsymbol{\mu}(0)\right]\right\rangle$. Figure 3(B) displays $r(t)$ probed at 2180 cm^{-1} for $CH_3SCN\cdots Li^+$ and at 2133 cm^{-1} for CH_3SCN, respectively. The orientational anisotropy decay, $r(t)$, was well fit by a bi-exponential function,

$$r(t) = b_1 \exp(-t/\tau_{or1}) + b_2 \exp(-t/\tau_{or2}) \quad (4)$$

where $\tau_{or1} < \tau_{or2}$. The fit results are summarized in Table 1. The orientational dynamics are bi-exponential with a fast component of a few ps and a slow component of tens of ps. The bi-exponential behavior of the orientational dynamics of small molecules is often explained by a wobbling-in-a-cone model.[40, 47, 48] The relative magnitudes of the fast and slow components are quite different for free CH_3SCN and $CH_3SCN\cdots Li^+$ complex. The slower component (τ_{or2}) of $r(t)$ is substantially different and measured to be 14±1 for CH_3SCN and 41±2 ps for $CH_3SCN\cdots Li^+$, respectively. This results from the fact that Li^+ ion has a relatively large charge density and thus can interact strongly with the surrounding solvent molecules by ion-dipole interactions, which slows down the orientational relaxation of $CH_3SCN\cdots Li^+$. In fact, the slow

component of $r(t)$ has been shown to be linearly dependent on the solution viscosity in the frame of the Debye-Stokes Einstein equation.[48]

D. Kinetic analysis of the complexation dynamics in T_w-dependent 2DIR spectra

The complexation dynamics of CH_3SCN and Li^+ observed in the T_w-dependent 2DIR spectra can be fully represented by the two-species exchange kinetics,

$$\xleftarrow[\text{decay}]{T_{1,F},\ \tau_{or,F}} \mathrm{CH_3SCN} + \mathrm{Li^+} \underset{k_d}{\overset{k_a}{\rightleftharpoons}} \mathrm{CH_3SCN \cdots Li^+} \xrightarrow[\text{decay}]{T_{1,C},\ \tau_{or,C}} \qquad \text{(Scheme 1)}$$

where k_a and k_d are the association (or complexation) and dissociation rate constants, $T_{1,F}$ and $T_{1,C}$ are the vibrational lifetimes, and $\tau_{or,F}$ and $\tau_{or,C}$ are the orientational relaxation times of free CH_3SCN and $CH_3SCN\cdots Li^+$, respectively. By using the two-species exchange kinetics, the coupled differential equations are set up in terms of the concentrations of the diagonal peaks and cross-peaks. By solving the coupled differential equations, the analytical solutions for the concentrations of the diagonal peaks and cross-peaks are obtained (See the ESI for details). For a quantitative analysis, all the peaks in 2DIR spectra are fitted by 2D Gaussian functions and their volumes are numerically calculated. The volumes of diagonal peaks and cross-peaks are plotted against T_w as data points in Figure 4(B). In this analysis, the volumes of individual peaks in 2DIR spectra are directly related to the concentrations of the corresponding species (i.e., $V_F \propto \mu_F^4 C_F$ and $V_C \propto \mu_C^4 C_C$, and $V_X \propto \mu_F^2 \mu_C^2 C_X$ where μ is the transition dipole moment of each species and is determined from the concentration-dependent FTIR spectra.). In the two-species exchange kinetic scheme, the orientational relaxation times ($\tau_{or,F}$ and $\tau_{or,C}$) were measured by polarization-controlled IR PP experiments as mentioned in the previous section. Finally, to determine the association and dissociation rate constants (k_a and k_d) as well as the true vibrational lifetimes ($T_{1,F}$ and $T_{1,C}$), the volumes of diagonal peaks and cross-peaks and $P(t)$ were simultaneous fitted by the analytical equations obtained from the two-species exchange

kinetics (see the ESI for details). The fitted results are the lines in Figures 4(B) and 4(C). The parameters determined from and used for the two-species exchange kinetic analyses are summarized in Table 2. First, the true vibrational lifetimes of the nitrile stretching vibration of CH_3SCN and $CH_3SCN\cdots Li^+$ are determined to be T_1= 80 and 95 ps, respectively, which are obviously different from the apparent lifetimes which are obtained by a single exponential fit to $P(t)$. Second, the dissociation and association time constants are determined to be $\tau_d=1/k_d=160\pm10$ ps and $\tau_a'=1/k_a'=1/k_a[Li^+]=360\pm20$ ps, respectively.

Before this section is closed, it should be mentioned that the concentration of CH_3SCN in this work is relatively high (1.69 M) and the intermolecular energy transfer among CH_3SCN molecules might contribute to the 2DIR signals. In 1.69 M CH_3SCN solution, the average intermolecular distance between CH_3SCN molecules is estimated to be approximately 20 angstroms. Generally, the intermolecular vibrational energy transfer is relatively efficient when the donor and accept are within a few angstroms and its efficiency is proportional to the distance between the donor and acceptor (i.e., $1/r^6$).[49] Under our experimental condition, the intermolecular vibrational energy transfer between CH_3SCN molecules could be safely neglected.

Recently, ion pairing dynamics between Li^+ and SCN^- ($Li^+ + SCN^- \rightleftharpoons$ Li-SCN) in dimethylformamide (DMF) were investigated by 2DIR spectroscopy and the dissociation time constant of Li-SCN ion pair was measured to be 190 ps, the association time constant was 165 ps.[4] The electrostatic interaction between Li^+ and SCN^- is expected to be quite different from the ion-dipole interaction between Li^+ and CH_3SCN. Direct comparison between two experimental results may not be conclusive because the ion pairing dynamics and complexation dynamics were investigated in different solvents (DMF *vs.* acetonitrile). However, the two experimental results indicate that both ion pairing dynamics between Li^+ and SCN^- and complexation dynamics between Li^+ and CH_3SCN occur on hundred picosecond timescales.

Such timescales should be important in understanding the dynamic properties of electrolyte solutions.

V. Summary and concluding remarks

To study the molecular dynamics by 2DIR spectroscopy, the vibrational probes with long lifetimes and spectral sensitivity are required. In this sense, CH_3SCN is proven to be an excellent vibrational probe because its nitrile stretching vibrational lifetime is ~90 ps in acetonitrile and its frequency is substantially blue-shifted by ~30 cm^{-1} when it forms $CH_3SCN\cdots Li^+$ complex. Such spectral properties of CH_3SCN can be used to directly measure the molecular dynamics occurring on hundred picosecond timescales. In this work, the complexation dynamics of CH_3SCN and Li^+ in acetonitrile were comprehensively studied by FTIR, IR PP, and 2DIR spectroscopy. Our temperature-dependent FTIR experimental results indicate that the complexation of CH_3SCN and Li^+ in acetonitrile is exothermic and entropically unfavorable. The complexation dynamics of CH_3SCN and Li^+ in acetonitrile are measured in real time by 2DIR spectroscopy and are found to occur on hundred picosecond timescales by. Such timescales are important in understanding the fluctuation of solvent configurations in ionic solvation shells and the diffusion of ions through polar channels or matrix. Ion-molecule complexation dynamics would depend on the interaction between ion and dipolar molecule, the solvent polarity, temperature, and so on. For example, the strength of the ion-dipole interaction can be varied by using the cations with different charge density and size. The solvent with different polarity or dielectric constant can influence on the ion-dipole complexation dynamics. Therefore, such systematic studies could provide more detailed information on the ion-molecule complexation dynamics.

Acknowledgements

This work was supported by the National Research Foundation of Korea (NRF) grants funded by the Korea government (MEST) (Nos. 2013R1A1A2009991 and 20100020209). The 2DIR and IR PP experiments were conducted in the Multidimensional Spectroscopy Laboratory at Korea Basic Science Institute (KBSI) Seoul Center.

References

1. J. M. G. Barthel, H. Krienke and W. Kunz, *Physical Chemistry of Electrolyte Solutions*, Springer, New York, 1998.
2. Y. Marcus and G. Hefter, *Chem. Rev.*, 2006, 106, 4585-4621.
3. K.-H. Park, S. R. Choi, J.-H. Choi, S. Park and M. Cho, *ChemPhysChem*, 2010, 11, 3632-3637.
4. K.-K. Lee, K.-H. Park, D. Kwon, J.-H. Choi, H. Son, S. Park and M. Cho, *J. Chem. Phys.*, 2011, 134, 064506.
5. J. Zheng, K. Kwak, J. Asbury, X. Chen, I. Piletic and M. D. Fayer, *Science*, 2005, 309, 1338-1343.
6. M. L. Cowan, B. D. Bruner, N. Huse, J. R. Dwyer, B. Chugh, E. T. J. Nibbering, T. Elsaesser and R. J. D. Miller, *Nature*, 2005, 434, 199.
7. J. Zheng, K. Kwak, J. Xie and M. D. Fayer, *Science*, 2006, 313, 1951-1955.
8. J. J. Loparo, S. T. Roberts and A. Tokmakoff, *J. Chem. Phys*, 2006, 125, 194522.
9. D. B. Strasfeld, Y. L. Ling, S.-H. Shim and M. T. Zanni, *J. Am. Chem. Soc.*, 2008, 130, 6698–6699.
10. Y. S. Kim and R. M. Hochstrasser, *J. Phys. Chem. B*, 2009, 113, 8231-8251.
11. S. Park, M. Odelius and K. J. Gaffney, *J. Phys. Chem. B.*, 2009, 113, 7825-7835
12. M. Ji, S. Park and K. J. Gaffney, *J. Phys. Chem. Lett.*, 2010, 1, 1771-1775.
13. R. A. Nicodemus, K. Ramasesha, S. T. Roberts and A. Tokmakoff, *J. Phys. Chem. Lett.* , 2010, 1, 1068-1072.
14. S. Park, M. Ji and K. J. Gaffney, *J. Phys. Chem. B*, 2010, 114, 6693-6702.
15. M. Ji, M. Odelius and K. J. Gaffney, *Science*, 2010, 328, 1003.
16. S. Park and M. Ji, *ChemPhysChem*, 2011, 12, 799-805.
17. H. T. Bian, X. W. Wen, J. B. Li, H. L. Chen, S. Z. Han, X. Q. Sun, J. A. Song, W. Zhuang and J. R. Zheng, *Proc. Nat. Acad. Sci. USA*, 2011, 108, 4737-4742.
18. J. T. King and K. J. Kubarych, *J. Am. Chem. Soc.*, 2012, 134, 18705-18712.
19. H. Son, D. Nam and S. Park, *J. Phys. Chem. B*, 2013, 117, 13604-13613.
20. Z. Getahun, C.-Y. Huang, T. Wang, B. D. León, W. F. DeGrado and F. Gai, *J. Am. Chem. Soc.*, 2003, 125, 405-411.
21. B. A. Lindquist, K. E. Furse and S. A. Corcelli, *Phys. Chem. Chem. Phys.*, 2009, 11, 8119-8132.
22. S. Bagchi, S. G. Boxer and M. D. Fayer, *J. Phys. Chem. B*, 2012, 116, 4034-4042.

23. M. M. Waegele, R. M. Culick and F. Gai, *J. Phys. Chem. Lett.*, 2012, 2, 2598-2609.
24. K.-H. Park, J. Jeon, Y. Park, S. Lee, H.-J. Kwon, C. Joo, S. Park, H. Han and M. Cho, *J. Phys. Chem. Lett.*, 2013, 4, 2105-2110.
25. V. Etacheri, R. Marom, R. Elazari, G. Salitra and D. Aurbach, *Energy Environ. Sci.*, 2011, 4, 3243-3262.
26. L. Suo, Y.-S. Hu, H. Li, M. Armand and L. Chen, *Nat. Comm.*, 2013, 4, 1481.
27. J. B. Goodenough and K.-S. Park, *J. Am. Chem. Soc.*, 2013, 135, 1167-1176.
28. K. Karthikeyan, S. Amaresh, V. Aravindan, H. Kim, K. S. Kang and Y. S. Lee, *J. Mater. Chem. A*, 2013, 1, 707-714.
29. A. Jain, V. Aravindan, S. Jayaraman, P. S. Kumar, R. Balasubramanian, S. Ramakrishna, S. Madhavi and M. P. Srinivasan, *Sci. Rep.*, 2013, 3, 3002.
30. V. Aravindan, J. Gnanaraj, Y.-S. Lee and S. Madhavi, *Chem. Rev.*, 2014, 114, 11619-11635.
31. H. Son, Y. Kwon, J. Kim and S. Park, *J. Phys. Chem. B* 2013, 117, 2748−2756.
32. D. Nam, C. Lee and S. Park, *Phys. Chem. Chem. Phys.*, 2014, 16, 21747-21754
33. C. Lee, D. Nam and S. Park, *New J. Chem.*, 2015, 39, 3520-3527.
34. M. C. Asplund, M. T. Zanni and R. M. Hochstrasser, *Proc. Natl. Acad. Sci. USA*, 2000, 97, 8219-8224.
35. M. Khalil, N. Demirdoeven and A. Tokmakoff, *J. Phys. Chem. A*, 2003, 107, 5258-5279.
36. I. J. Finkelstein, J. Zheng, H. Ishikawa, S. Kim, K. Kwak and M. D. Fayer, *Phys. Chem. Chem. Phys.*, 2007, 9, 1533-1549.
37. S.-H. Shim and M. T. Zanni, *Phys. Chem. Chem. Phys.*, 2007, 11, 748-761.
38. S. Park and M. D. Fayer, *Proc. Natl. Acad. Sci. USA*, 2007, 104, 16731-16738.
39. S. Park, K. Kwak and M. D. Fayer, *Laser Phys. Lett.*, 2007, 4, 704-718.
40. S. Park, D. E. Moilanen and M. D. Fayer, *J. Phys. Chem. B*, 2008, 102, 5279-5290.
41. P. Hamm and M. Zanni, *Concepts and Methods of 2D Infrared Spectroscopy* Cambridge University Press, UK, 2011.
42. M. Khalil, N. Demirdoven and A. Tokmakoff, *Phys. Rev. Lett.*, 2003, 90, 047401(047404).
43. D. E. Moilanen, N. Levinger, D. B. Spry and M. D. Fayer, *J. Am. Chem. Soc.*, 2007, 129, 14311-14318.
44. M. G. Maienschein-Cline and C. H. Londergan, *J. Phys. Chem. A*, 2007, 111, 10020-10025.

45. W. Rock, Y.-L. Li, P. Pagano and C. M. Cheatum, *J. Phys. Chem. A*, 2013, 117, 6073-6083.
46. L. J. G. W. v. Wilderen, D. Kern-Michler, H. M. Müller-Werkmeister and J. Bredenbeck, *Phys. Chem. Chem. Phys.*, 2014, 16, 19643-19653.
47. K. J. Gaffney, I. R. Piletic and M. D. Fayer, *J. Chem. Phys.*, 2003, 118, 2270-2278.
48. H. Son, J. Haneul, S. R. Choi, H. W. Jung and S. Park, *J. Phys. Chem. B*, 2012, 116, 9152-9159.
49. H. Chen, X. Wen, X. Guo and J. Zheng, *Phys. Chem. Chem. Phys.*, 2014, 16, 13995-14014.

Table 1. Exponential fit to the population decay, *P*(*t*), and orientational anisotropy, *r*(*t*).

	Freq. (cm^{-1})	T_1 (ps)	b_1	τ_{or1} (ps)	b_2	τ_{or2} (ps)
CH_3SCN ($\upsilon = 1 \rightarrow 2$)	2133	92±2	0.23±0.02	2.4±0.2	0.11±0.01	14±1
$CH_3SCN\cdots Li^+$ ($\upsilon = 0 \rightarrow 1$)	2180	78±2	0.06±0.01	5.1±0.3	0.32±0.02	41±2

Table 2. Parameters determined from and used for the two-species exchange kinetic analysis.

	T_1 (ps)[a]	τ_{or} (ps)[b]	Relative μ_{01}	Relative Conc.	$\tau_d=1/k_d$ (ps)	$\tau_a'=1/k_a'$ (ps)	$\tau_{ex}=1/k_{ex}$ (ps)
CH_3SCN	80	6.2	1.0	1.0	160±10	360±20	110±10
$CH_3SCN\cdots Li^+$	95	36	1.35	0.43			

[a] True vibrational lifetimes obtained from the two-species exchange kinetic analysis.
[b] Orientational relaxation times obtained by a single exponential fit to *r*(*t*).

Figure captions

Figure 1. (A) Nitrile stretch band of CH_3SCN (1.69 M) at different concentrations of Li^+. (B) Nitrile stretch band of CH_3SCN (1.69 M) with Li^+ (2.0 M) at different temperatures. (C) Decomposition of FTIR spectrum measured at 30 °C into the nitrile stretch bands of CH_3SCN and $CH_3SCN\cdots Li^+$. The areas under the decomposed peaks are calculated. (D) The van't Hoff plot is shown and it provides information on the enthalpy (ΔH) and entropy (ΔS) for the complexation equilibrium between CH_3SCN and Li^+.

Figure 2. 2DIR spectra of CH_3SCN and Li^+ in acetonitrile with increasing T_w. 2DIR spectra are normalized by the maximum peak at each T_w. The diagonal axis is indicated by dotted line. At T_w=180 ps, Peak F and C on the diagonal represent the nitrile stretching peak of CH_3SCN and $CH_3SCN\cdots Li^+$, respectively, Peak X1, X2, and X3 represent the cross-peaks. As T_w is increased, the cross-peaks (X1, X2, and X3) grow gradually due to the complexation equilibrium between CH_3SCN and Li^+.

Figure 3. Polarization-controlled IR PP experimental results. (A) Population decays, $P(t)$, of the nitrile stretch vibration of free CH_3SCN and $CH_3SCN\cdots Li^+$ complex. The lines are a single exponential fit. (B) Orientational anisotropy decays, $r(t)$, of free CH_3SCN and $CH_3SCN\cdots Li^+$ complex. The lines are a bi-exponential fit.

Figure 4. (A) Two-species exchange kinetics observed in the T_w-dependent 2DIR spectra. (B) The volumes of the diagonal (C and F) peaks and cross-peak (X) are plotted against T_w. (C) $P(t)$ obtained from polarization-controlled IR PP experiments. In (B) and (C), the peak volumes and $P(t)$ are simultaneously fitted to the two-species exchange kinetics to determine the rate constants and vibrational lifetimes.

.

Figure 1

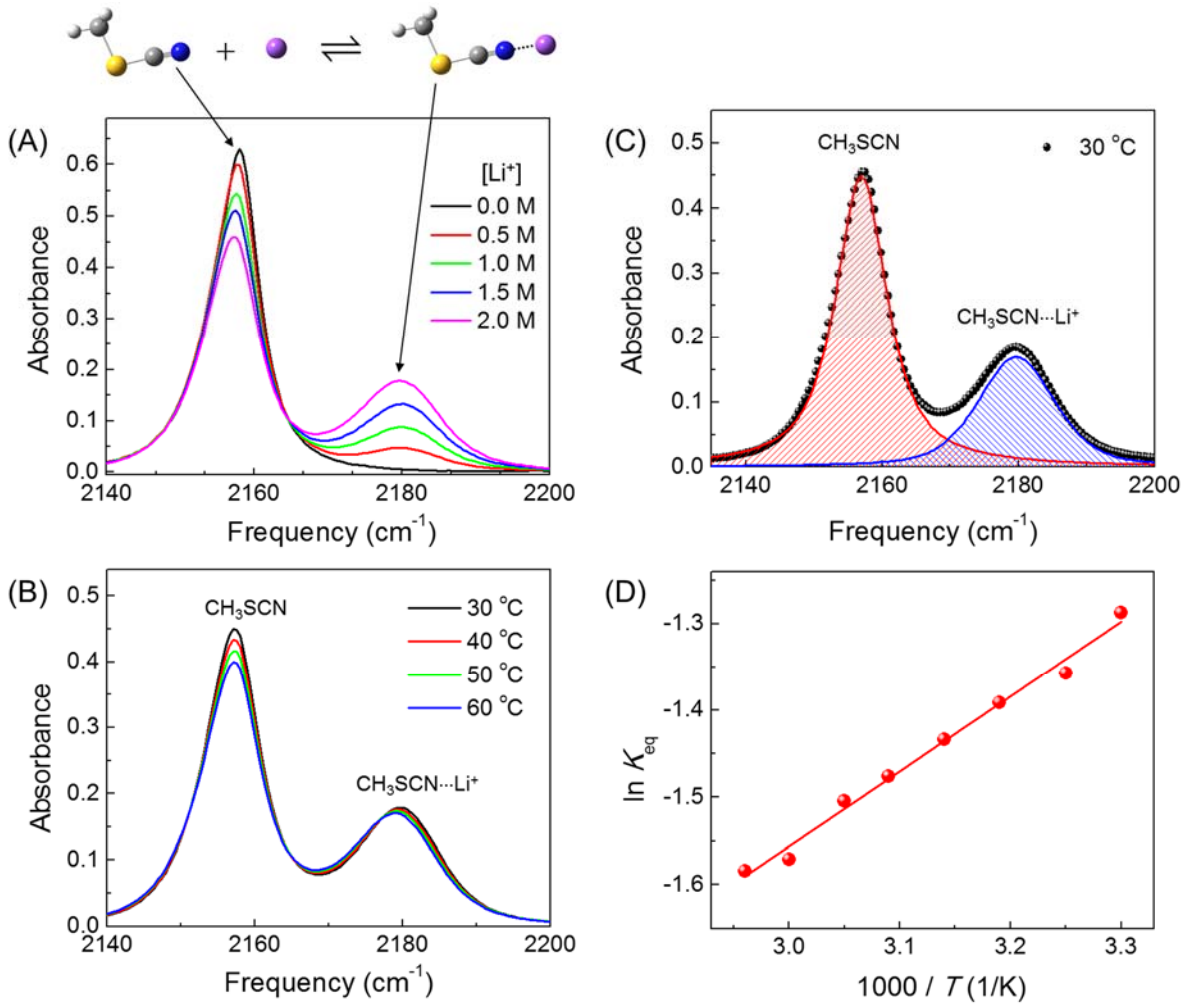

Figure 1. (A) Nitrile stretch band of CH_3SCN (1.69 M) at different concentrations of Li^+. (B) Nitrile stretch band of CH_3SCN (1.69 M) with Li^+ (2.0 M) at different temperatures. (C) Decomposition of FTIR spectrum measured at 30 °C into the nitrile stretch bands of CH_3SCN and $CH_3SCN\cdots Li^+$. The areas under the decomposed peaks are calculated. (D) The van't Hoff plot is shown and it provides information on the enthalpy (ΔH) and entropy (ΔS) for the complexation equilibrium between CH_3SCN and Li^+.

Figure 2

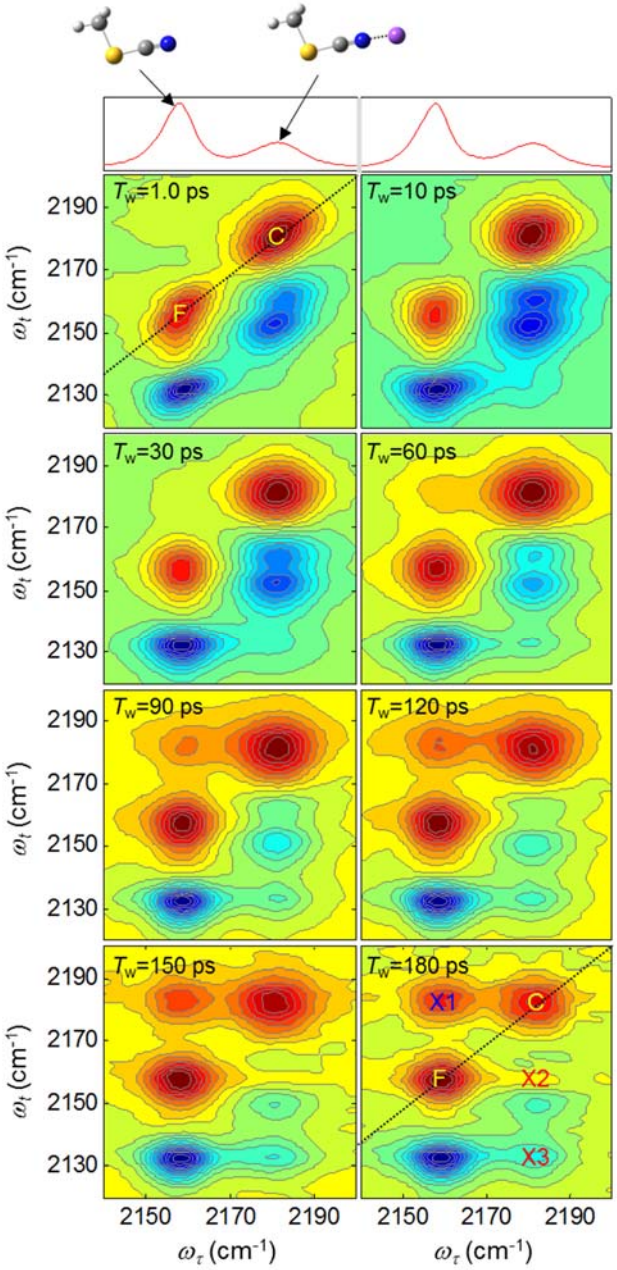

Figure 2. 2DIR spectra of CH_3SCN and Li^+ in acetonitrile with increasing T_w. 2DIR spectra are normalized by the maximum peak at each T_w. The diagonal axis is indicated by dotted line. At T_w=180 ps, Peak F and C on the diagonal represent the nitrile stretching peak of CH_3SCN and $CH_3SCN\cdots Li^+$, respectively, Peak X1, X2, and X3 represent the cross-peaks. As T_w is increased, the cross-peaks (X1, X2, and X3) grow gradually due to the complexation equilibrium between CH_3SCN and Li^+.

Figure 3

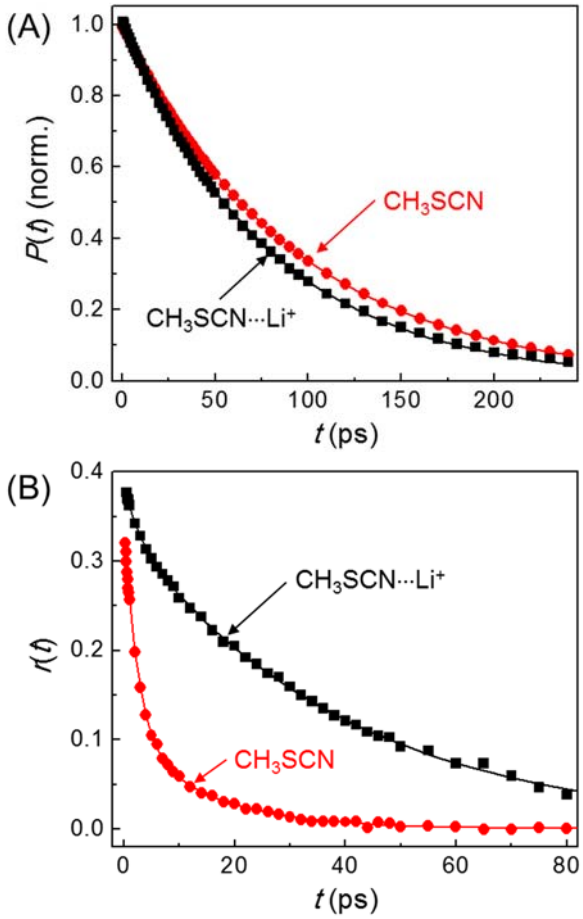

Figure 3. Polarization-controlled IR PP experimental results. (A) Population decays, $P(t)$, of the nitrile stretch vibration of free CH_3SCN and $CH_3SCN\cdots Li^+$ complex. The lines are a single exponential fit. (B) Orientational anisotropy decays, $r(t)$, of free CH_3SCN and $CH_3SCN\cdots Li^+$ complex. The lines are a bi-exponential fit.

Figure 4

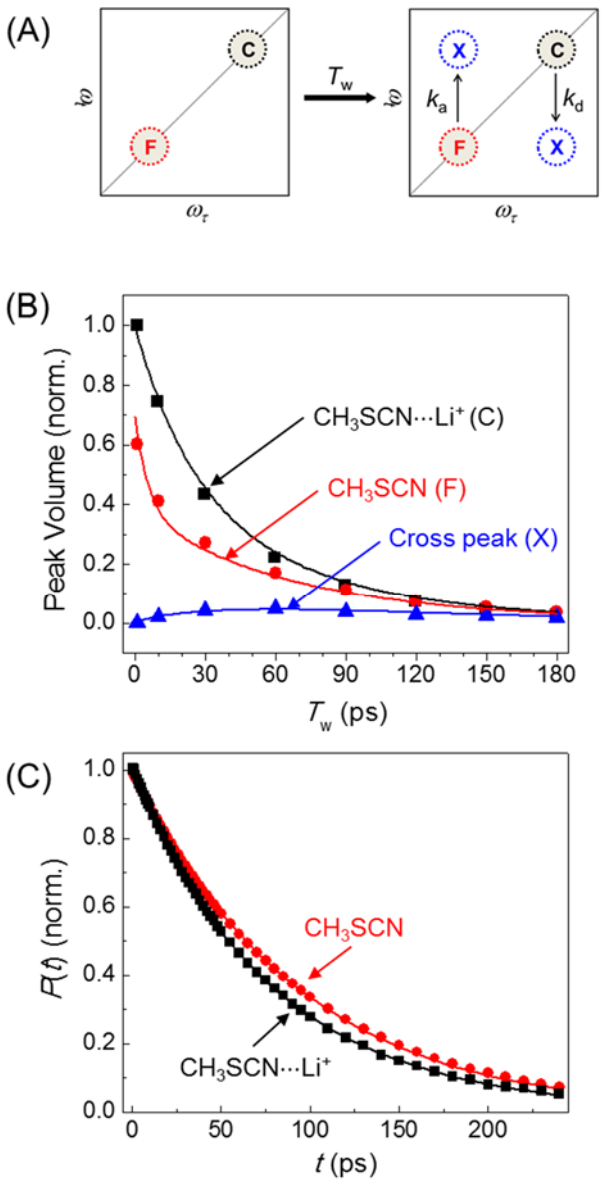

Figure 4. (A) Two-species exchange kinetics observed in the T_w-dependent 2DIR spectra. (B) The volumes of the diagonal (C and F) peaks and cross-peak (X) are plotted against T_w. (C) $P(t)$ obtained from polarization-controlled IR PP experiments. In (B) and (C), the peak volumes and $P(t)$ are simultaneously fitted to the two-species exchange kinetics to determine the rate constants and vibrational lifetimes.